Inorganic Chemistry

Article

Integration of Electron Density and Molecular Orbital Techniques to Reveal Questionable Bonds: The Test Case of the Direct Fe–Fe Bond in Fe$_2$(CO)$_9$

Joachim Reinhold,*,[†] Oliver Kluge,[†] and Carlo Mealli*,[‡]

Wilhelm-Ostwald-Institut für Physikalische und Theoretische Chemie, Universität Leipzig, D-04103 Leipzig, Germany, and Istituto di Chimica dei Composti Organo Metallici (ICCOM), CNR, I-50019 Sesto Fiorentino, Firenze, Italy

The article illustrates the advantages of partitioning the total electron density $\rho(r_b)$, its Laplacian $\nabla^2\rho(r_b)$, and the energy density $H(r_b)$ in terms of orbital components. By calculating the contributions of the mathematically constructed molecular orbitals to the measurable electron density, it is possible to quantify the bonding or antibonding character of each MO. This strategy is exploited to review the controversial existence of direct Fe–Fe bonding in the triply bridged Fe$_2$(CO)$_9$ system. Although the bond is predicted by electron counting rules, the interaction between the two pseudo-octahedral metal centers can be repulsive because of their fully occupied t$_{2g}$ sets. Moreover, previous atoms in molecules (AIM) studies failed to show a Fe–Fe bond critical point (bcp). The present electron density orbital partitioning (EDOP) analysis shows that one σ bonding combination of the t$_{2g}$ levels is not totally overcome by the corresponding σ* MO, which is partially delocalized over the bridging carbonyls. This suggests the existence of some, albeit weak, direct Fe–Fe bonding.

Introduction

Bonding is a fundamental aspect of chemistry. Whereas the shared-shell interactions between light atoms (common covalent or polar bonds) are usually well understood, the closed-shell interactions and the bonds between heavy atoms are less defined. Longstanding issues on the subject are still open, also in view of the numerous theoretical analyses and the sophisticated experimental approaches to the problem. For these reasons, the characterization of the chemical bond is not a closed subject.[1]

The reciprocal validation of atoms in molecules (AIM)[2] and molecular orbital (MO) approaches in bonding analyses is largely debated.[3–7] These methods are intrinsically different, because MOs imply the definition of the wave function ψ, whereas AIM is related to the magnitude ψ*ψ. From the latter, the electron density is derived by integration over the coordinates of all of the electrons except one. Importantly, the electron density has the advantage of being a measurable quantity, whereas the wave function is not. On the other hand, the wave function, based on some widely accepted approximations of quantum chemistry, determines the complex MO architecture. The latter is the general basis for most interpretations of the electron distribution and bond properties in molecules. Incidentally, a parallel difference exists in X-ray crystallography between the appropriately phased structure factors and the intensities of the reflections. In fact, the solution of a molecular structure does not descend directly from the latter observed magnitudes but requires appropriate modeling of the available chemical information or the usage of probabilistic methods to solve the phase problem. In the procedure, the electron contributions of the different atoms are added up to compute the final intensities.

---

* To whom correspondence should be addressed. E-mail: reinhold@chemie.uni-leipzig.de (J.R.), mealli@iccom.cnr.it (C.M.).

† Universität Leipzig.

‡ ICCOM, CNR.

(1) Coppens, P. *Angew. Chem., Int. Ed.* **2005**, *44*, 6810–6811.
(2) Bader, R. F. W. *Atoms in Molecules: A Quantum Theory*, Oxford University Press: Oxford, U.K., 1990.
(3) Gillespie, R. J.; Popelier, P. L. A. *From Lewis to Electron Densities*; Oxford University Press: New York, 2001.
(4) Frenking, G. *Angew. Chem., Int. Ed.* **2003**, *42*, 143–147.
(5) Bader, R. F. W. *Int. J. Quantum Chem.* **2003**, *94*, 173–177.
(6) Proceedings of the Euresco Conference on *New Theoretical and Spectroscopic Approaches to Inorganic Chemistry Problems* (chair-persons C. Mealli and S. Alvarez), Sant Feliu du Guixol (Spain), 2004 (http://www.esf.org/euresco/04/pc04018).
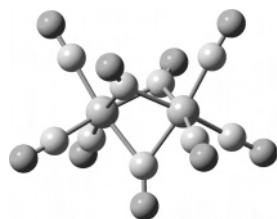(7) Cortés-Guzmán, F.; Bader, R. F. W. *Coord. Chem. Rev.* **2005**, *249*, 633–662.

Figure 1. Structure of $Fe_2(CO)_9$.

Topological studies of electron density, performed with the AIM method, allow us to distinguish between different types of atomic interactions. An exhaustive classification of the latter has been recently presented,[8] which summarizes the schemes of Bader,[2,9] Espinosa et al.,[10] and Macchi et al.[11,12] In most cases, the situation for shared-shell interactions between light atoms is well understood. At the bond critical point (bcp) r_b, the electron density $\rho(r_b)$ is large and the associated Laplacian $\nabla^2\rho(r_b)$ and energy density $H(r_b)$ values are significantly negative (these magnitudes will be specifically addressed in this article).

Complications arise in the AIM analysis of nontrivial atomic interactions, for example between metal atoms, for which subsidiary theoretical tools may be necessary. Thus, we propose in this article an electron density orbital partitioning (EDOP) analysis to highlight direct M−M interactions in bridged transition-metal carbonyls. The validity of this approach, which was recently introduced in the study of the bent Co−Co bond in $Co_2(CO)_8$,[13,14] is here confirmed by the rational answer provided to the aged and highly questioned problem of the direct Fe−Fe bond in the triply bridged system $Fe_2(CO)_9$ (Figure 1). Such a bond is predicted by chemical intuition and the powerful 18-electron rule, but its existence remains controversial after a number of theoretical analyses,[15−18] some of which have even suggested a prevailing repulsion between the two pseudo-octahedral metal centers with populated t_{2g} sets.[19] On the other hand, a careful interpretation of the entire MO structure, through simple symmetry and perturbation theory arguments,[20] pointed out the possible source of the direct Fe−Fe bonding interaction.[20] This would be due to the noncomplete cancellation of one σ bonding combination of the t_{2g} levels by the corresponding σ^* MO, which is partially delocalized over the bridging carbonyls. The picture received

further support from a series of ab initio optimizations of consistent $M_2(CO)_9$ model systems with M belonging to different groups. Thus, a variable number of electrons is permitted for evaluating the character and contribution of the critical frontier MOs.[21] A similar conclusion in favor of the direct Fe−Fe bonding is now reached by applying the EDOP analysis to $Fe_2(CO)_9$.

Results and Discussion

Electron Density Orbital Partitioning. The proposed orbital partitioning of the electron density applies to single-configuration wave functions derived from Hartree−Fock or state-of-the-art density functional theory (DFT) methods.[14] The partitioning is inapplicable if the electron correlation is treated through a configuration interaction. At the DFT level, however, the latter is semiempirically evaluated by retaining the single-determinant structure of the wave function. In summary, by performing a state-of-the-art DFT calculation, which is intrinsically based on the electron density, one obtains wave functions, that is, a set of MOs with certain occupation numbers. The latter are then used to calculate the electron density necessary to perform AIM studies. Obviously, the quality of the molecular wave functions depends on the chosen functional (e.g., B3LYP) and basis set, but this should not greatly affect the qualitative relationship between the total electron density at a given bond and the bonding/antibonding characters of the contributing MOs.

In the case of a single-configuration wave function, the total molecular densities [namely, the electron density $\rho(r)$, its Laplacian $\nabla^2\rho(r)$, and the energy density $H(r)$] are obtained by summing up the contributions from all of the occupied MOs. As it will be shown, important information is derived from these individual contributions and not only from the total densities that are used to determine complex bonding properties. For instance, a negative sign of the Laplacian, computed for a given MO at a specific space region, indicates local charge concentration, hence a bonding contribution of the MO in question to the total density. In contrast, a positive sign indicates local charge depletion, hence an antibonding contribution. Also, in agreement with the ideas of Cremer and Kraka,[22,23] the energy density $H(r)$ minimizes with a negative value, wherever there is the highest contribution of a given MO to the bonding energy.

Density Partitioning in $Fe_2(CO)_9$. A previous application of the classic AIM method to $Fe_2(CO)_9$ did not detect any Fe−Fe bcps.[18] As in other similar cases, the problem may arise from the significant amount of the electron density, which is redirected from the intermetallic region toward the CO ligands.[12] Also, the existence of a bcp may depend on the M−M separation (if this is stretched by the bridges)[24] and also on the quality of the basis set (below). However, even if the bcp is absent, a positive AIM-based delocalization

(8) Gatti, C. *Z. Kristallografiya* **2005**, *220*, 399−457.
(9) Bader, R. F. W.; Essén, H. *J. Chem. Phys.* **1984**, *80*, 1943−1960.
(10) Espinosa, E.; Alkorta, I.; Elguero, J.; Molins, E. *J. Chem. Phys.* **2002**, *117*, 5529−5542.
(11) Macchi, P.; Proserpio, D. M.; Sironi, A. *J. Am. Chem. Soc.* **1998**, *120*, 13429−13435.
(12) Macchi, P.; Sironi, A. *Coord. Chem. Rev.* **2003**, *238−239*, 383−412.
(13) Finger, M.; Reinhold, J. *Inorg. Chem.* **2003**, *42*, 8128−8130.
(14) Kluge, O.; Finger, M.; and Reinhold, J. *Inorg. Chem.* **2005**, *44*, 6494−6496.
(15) Heijser, W.; Baerends, E. J.; Ros, P. *Faraday Symp. Chem. Disc.* **1980**, *14*, 211−234.
(16) Bauschlicher, C. W., Jr. *J. Chem. Phys.* **1986**, *84*, 872−875.
(17) Rosa, A.; Baerends, E. J. *New J. Chem.* **1991**, *15*, 815−829.
(18) Bo, C.; Sarasa, J.-P.; Poblet, J.-M. *J. Phys. Chem.* **1993**, *97*, 6362−6366.
(19) Summerville, R. H.; Hoffmann, R. *J. Am. Chem. Soc.* **1979**, *101*, 3821−3831.
(20) Mealli, C.; Proserpio, D. M. *J. Organomet. Chem.* **1990**, *386*, 203−208.

(21) Reinhold, J.; Hunstock, E.; Mealli, C. *New J. Chem.* **1994**, *18*, 465−471.
(22) Cremer, D.; Kraka, E. *Angew. Chem., Int. Ed. Engl.* **1984**, *23*, 627−628.
(23) Cremer, D.; Kraka, E. *Croat. Chem. Acta* **1984**, *57*, 1259−1281.
(24) Phillips, A. D.; Ienco, A.; Reinhold, J.; Böttcher, H.-C.; Mealli, C. *Chem.—Eur. J.* **2006**, *12*, 4691−4701.

index (δ_{M-M}) can still underline an attractive interaction.[25,26] This index is usually consistent with the more classic Mayer bond order.[27,28] As an anticipation, the significantly positive value of the latter index for Fe–Fe in $Fe_2(CO)_9$ (+0.4, as obtained from the present DFT calculations) underlines the presence of an intermetallic bond and encourages us to look for its origin.

In this study, all of the AIM-type calculations were performed by using the Extreme routine of the Aimpac package,[29] with the DFT-B3LYP[30-32] calculated wave functions[33] as an input. To evaluate the contribution from single or grouped MOs, all of the occupation numbers were zeroed except for those of interest. Because of the mentioned difficulty in detecting the Fe–Fe bcp,[12] various different basis sets were tested (Supporting Information). For the less extended Fe basis sets and consistent with previous studies,[18] a cage critical point (ccp) is detected. This is characterized as a local minimum of the electron density that indicates an overall gluing of the atoms forming the central Fe_2C_3 bipyramid, but nothing specifies about the direct Fe–Fe bonding. By using more extended Fe basis sets, such as the Wachters+f one,[34,35] a Fe–Fe bcp becomes detectable. The present analysis is based on this Fe basis set (together with the 6-31G(d) one[36] for the C and O atoms), also because of the excellent match between the optimized and experimental[37] structures (maximum deviations <1 pm and 1°, Supporting Information).

All of the values of $\rho(r)$, $\nabla^2\rho(r)$, and $H(r)$, which appear in Figure 2, were analyzed along one of the three equivalent

(25) The index $\delta_{A-B} = F(A,B) + F(B,A)$ measures the extent of electron exchange or sharing between two adjacent atomic basins A and B. $F(A,B) = F(B,A)$ represents the combined summation of the S_{ij} elements of the atomic overlap matrix $-\sum_i\sum_j S_{ij}(A)S_{ij}(B)$.
(26) Bader, R. F. W.; Stephens, M. E. *J. Am. Chem. Soc.* **1975**, 97, 7391–7399.
(27) The Mayer index is defined as $\beta_{A-B} = -\sum_i\sum_j(PS)_{ij}(PS)_{ji}$, where P is the density matrix and S is the overlap matrix of the atomic orbitals.
(28) Mayer, I. *Chem. Phys. Lett.* **1983**, 97, 270–274.
(29) Biegler-König, F. W.; Bader, R. F. W.; Tang, T.-H. *J. Comput. Chem.* **1982**, 3, 317–328.
(30) Becke, A. D. *J. Chem. Phys.* **1993**, 98, 5648–5652.
(31) Lee, C.; Yang, W.; Parr, R. G. *Phys. Rev.* **1988**, B37, 785–789.
(32) Vosko, S. J.; Wilk, L.; Nusair, M. *Can. J. Phys.* **1980**, 58, 1200–1211.
(33) Frisch, M. J.; Trucks, G. W.; Schlegel, H. B.; Scuseria, G. E.; Robb, M. A.; Cheeseman, J. R.; Montgomery, J. A., Jr.; Vreven, T.; Kudin, K. N.; Burant, J. C.; Millam, J. M.; Iyengar, S. S.; Tomasi, J.; Barone, V.; Mennucci, B.; Cossi, M.; Scalmani, G.; Rega, N.; Petersson, G. A.; Nakatsuji, H.; Hada, M.; Ehara, M.; Toyota, K.; Fukuda, R.; Hasegawa, J.; Ishida, M.; Nakajima, T.; Honda, Y.; Kitao, O.; Nakai, H.; Klene, M.; Li, X.; Knox, J. E.; Hratchian, H. P.; Cross, J. B.; Adamo, C.; Jaramillo, J.; Gomperts, R.; Stratmann, R. E.; Yazyev, O.; Austin, A. J.; Cammi, R.; Pomelli, C.; Ochterski, J. W.; Ayala, P. Y.; Morokuma, K.; Voth, G. A.; Salvador, P.; Dannenberg, J. J.; Zakrzewski, V. G.; Dapprich, S.; Daniels, A. D.; Strain, M. C.; Farkas, O.; Malick, D. K.; Rabuck, A. D.; Raghavachari, K.; Foresman, J. B.; Ortiz, J. V.; Cui, Q.; Baboul, A. G.; Clifford, S.; Cioslowski, J.; Stefanov, B. B.; Liu, G.; Liashenko, A.; Piskorz, P.; Komaromi, I.; Martin, R. L.; Fox, D. J.; Keith, T.; Al-Laham, M. A.; Peng, C. Y.; Nanayakkara, A.; Challacombe, M.; Gill, P. M. W.; Johnson, B.; Chen, W.; Wong, M. W.; Gonzalez, C.; Pople, J. A. *Gaussian 03*, Revision C.02, Gaussian, Inc., Pittsburgh, PA, 2003.
(34) Wachters, A. J. H. *J. Chem. Phys.* **1970**, 52, 1033–1036.
(35) Bauschlicher, C. W., Jr.; Langhoff, S. R.; Partridge, H.; Barnes, L. A. *J. Chem. Phys.* **1989**, 91, 2399–2411.
(36) Hehre, W. J.; Radom, L.; Schleyer, P. v. R.; Pople, J. A. *Ab initio Molecular Orbital Theory*; Wiley & Sons: New York, 1986.
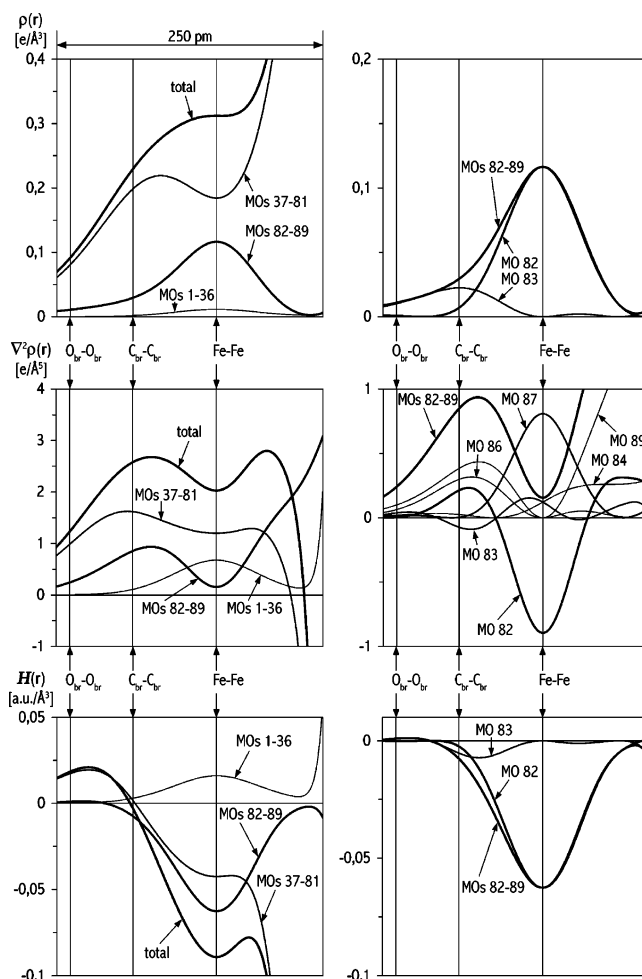(37) Cotton, F. A.; Troup, J. M. *J. Chem. Soc., Dalton Trans.* **1974**, 800–802.

Figure 2. Boxes show, in top-down order, the variations of the electron density, its Laplacian, and the energy density along one of the 2-fold axes of $Fe_2(CO)_9$ [B3LYP, Wachters+f basis set for the Fe atoms and the 6-31g-(d) basis set for the others]. On the left side, the bold lines refer to the total densities, whereas the gray lines represent the contributions of different MO groups. On the right side, the contributions of the frontier orbital group (MOs 82–87) are repeated on a different scale (bold lines) together with those of the individual orbitals (gray lines), which are depicted in Figure 3. The vertical lines are key reference points along the 2-fold axis (Figure 1 and the text).

2-fold symmetry axes of the D_{3h} molecule $Fe_2(CO)_9$. The vertical lines in each diagram indicate, in left to right order, the projections of the two O and the two C atoms, which do not lie on the selected axis, and the intersection of the latter with the Fe–Fe vector. The atoms of the third bridging CO (on the axis) lie out of scale at the right side of each diagram.

The total densities appear as bold lines in the left-side boxes. Notice that, in the top-left box, the total electron density reaches a flat plateau in the core center. Actually, there is a slight maximum at the intersection with the Fe–Fe vector, that is, in correspondence with the observed bcp ($\rho(r_c) = 0.31$ e/Å³). As mentioned, the usage of less extended Fe basis sets causes a minimum of $\rho(r)$ at the Fe–Fe intersection, which corresponds to a ccp. Although the nature of the critical point depends on the basis set (and likely also on the functional used), a comparison of the data in Table 2 of the Supporting Information shows that the density values at the Fe–Fe midpoint are similar in all cases, and the shape of the total electron density curve is only marginally

Table 1. Comparison of Experimental and Optimized Distances and Angles (pm and Deg) in $Fe_2(CO)_9$[a]

	exptl [37]	compd
Fe−Fe	252.3	253.0
Fe−C_{br}	201.6	200.9
Fe−C_t	183.8	183.6
C_{br}−O_{br}	117.6	117.2
C_t−O_t	115.6	114.8
Fe−Fe−C_t	120.9	120.5
Fe−C_t−O_t	177.1	177.6

[a] All the computed values are based on DFT-B3LYP calculations with Wachters+f[34,35] basis set for Fe and the 6-31G(d)[36] basis set for C and O.

Table 2. Characteristics of the Critical Point between the Iron Atoms of $Fe_2(CO)_9$ in Dependence on the Basis Sets

Fe	C and O		$\rho(r_c)$ [e$Å^{-3}$]	$\nabla^2\rho(r_c)$ [e$Å^{-5}$]	$H(r_c)$ [au $Å^{-3}$]
3-21G [36]	3-21G	ccp	0.23	4.0	0.04
6-31G [36]	6-31G	bcp	0.29	2.3	−0.08
LANL2DZ [a]	6-31G(d)	ccp	0.26	3.5	0.01
6-31G(d)	6-31G(d)	bcp	0.30	2.4	−0.08
6-311G(d) [36]	6-311G(d)	bcp	0.30	2.6	−0.06
Ahlrichs TZV [b]	6-31G(d)	bcp	0.29	2.9	−0.04
Ahlrichs TZV	6-311G(d)	ccp	0.29	3.0	−0.03
Wachters+f [34,35]	6-31G(d)	bcp	0.31	2.0	−0.09
Wachters+f	6-311G(d)	bcp	0.31	2.1	−0.09
WTBS [c]	6-31G(d)	ccp	0.25	3.1	−0.01
WTBS	6-311G(d)	ccp	0.25	3.1	−0.01

[a] Hay, P. J.; Wadt, W. R. *J. Chem. Phys.* **1985**, *82*, 270−283, 284−298, 299−310. [b] Schäfer, A.; Huber, C.; Ahlrichs, R. *J. Chem. Phys.* **1994**, *100*, 5829−5835. [c] Huzinaga, S.; Miguel, B. *Chem. Phys. Lett.* **1990**, *175*, 289−291; Huzinaga, S.; Klobukowski, M. *Chem. Phys. Lett.* **1993**, *212*, 260−264.

influenced by the nature of the critical point. In fact, there is always a rather flat plateau with a very weak maximum or minimum at the Fe−Fe midpoint, which corresponds to a bcp or a ccp, respectively. In the latter case, the maximum is slightly shifted to the left.

The total energy density (bottom-left box) reaches a negative minimum at the Fe−Fe intersection ($H(r_c) = -0.09$ au/$Å^3$), where there is also a positive minimum of the total Laplacian ($\nabla^2\rho(r_c) = 2.1$ e/$Å^5$). Altogether, the quantitative information emerging from classical AIM tools and based on the total densities appears contradictory because the depletion of the charge density (positive Laplacian) points to a closed-shell interaction. However, an improvement of the basis set with the detection of the bcp seems to change the interaction from repulsive to attractive and leaves the existence of the Fe−Fe bond uncertain.

The following orbital partitioning analysis provides a reasonable explanation for such a global response of the AIM method. To this purpose, Figure 2 also presents selected contributions from single or grouped orbitals. For a quick reference, all of the 89 filled MOs are scaled, in three different groups, at the left side of Figure 3. The contributions of these groups to $\rho(r)$, $\nabla^2\rho(r)$, and $H(r)$ are included in the corresponding left-side boxes of Figure 2. The inner shells (MOs 1−36) have little weight in the total charge density within the $Fe_2(\mu\text{-}CO)_3$ region. Moreover, the flat and positive maxima of the corresponding $\nabla^2\rho(r)$ and $H(r)$ curves indicate the repulsive interaction between these inner shells. The second group is formed by MOs 37−81, with prevailing

intraligand and Fe−(CO)$_{terminal}$ bonding characters. Also, this group includes the bonding combinations between the σ donor orbitals at the CO bridges and metal acceptor orbitals, which account for three of the six Fe−(CO)$_{bridge}$ bonds. Essentially, the positive maxima of $\nabla^2\rho(r)$ and $H(r)$ (central and bottom-left boxes) are indicative of repulsive interactions between the two CO bridges, which are not on the selected axis. Notice, however, that at the Fe−Fe intersection (i.e., at the bcp), $H(r)$ is negative thus suggesting a net weak attractive contribution due to these levels.

Finally, the attention is focused on frontier MOs 82−89. For the latter, the group contributions to $\rho(r)$, $\nabla^2\rho(r)$, and $H(r)$ are repeated, on different scales, in the right-side boxes (bold lines) together with single MO contributions. Figure 3 shows the drawings of all of these MOs. The HOMO and HOMO$_{-1}$ (88−89) are the back-bonding combinations between occupied d$_\pi$ metal orbitals and empty CO π^* levels;[19,20] hence, they account for the formation of two additional Fe−(CO)$_{bridge}$ bonds. The remaining MOs 82−87 are, in principle, the *in-phase* and *out-of-phase* combinations of the formally nonbonding t$_{2g}$ sets of the two pseudo-octahedral metal centers.

MO group 82−89 deserves further attention, because it seems largely responsible for the appearance of the bcp and the negative minimum of the energy density. In particular, these features are mainly imposed by MO 82 (d$_\sigma$−d$_\sigma$ in character), with a very small influence of MO 83 (d$_\delta$−d$_\delta$ character). In fact, all of the remaining levels give, in view of their nodal properties, only vanishing contributions to ρ-(r) and $H(r)$. As shown in the bottom-left box of Figure 2, the energy density contribution of groups 82−89 (hence, essentially of MO 82) is larger than that of all lower levels 37−81 with mainly ligand character. This explains why the Fe−Fe bcp is so sensitive to the metal basis set.

The Direct Interactions Between the Two Fe Centers. Because occupied MO 87 represents the σ^* counterpart of σ level 82, an electron-pair repulsion should be active, instead of having a net Fe−Fe bonding effect. In principle, this behavior of the orbital pair may not be adequately reflected by either the charge density $\rho(r)$ or the energy density $H(r)$ at the bcp, because the respective values for MO 87 (and others) vanish on account of the nodal properties. To understand this argument better, the simple, yet unrealistic, model with two He atoms at the arbitrarily fixed short distance of 75 pm was considered (Figure 4). In analogy with the previous picture, a bcp is observed with a correspondingly negative $H(r_c)$ value. This is because only the σ and not the σ^* level contributes to the electron and energy densities on the mirror plane between the two atoms. On the other hand, because $H(r_c)$ is found to increase with the interatomic separation, an adequate concentration of the σ charge density (hence, stabilizing energetics) is possible only beyond a lower limit of the He−He distance. Conversely, the Laplacian (central box in Figure 4) shows how the large depletion of the electron density associated with σ^* over-compensates the concentration because of σ. Indeed, $\nabla^2\rho$-
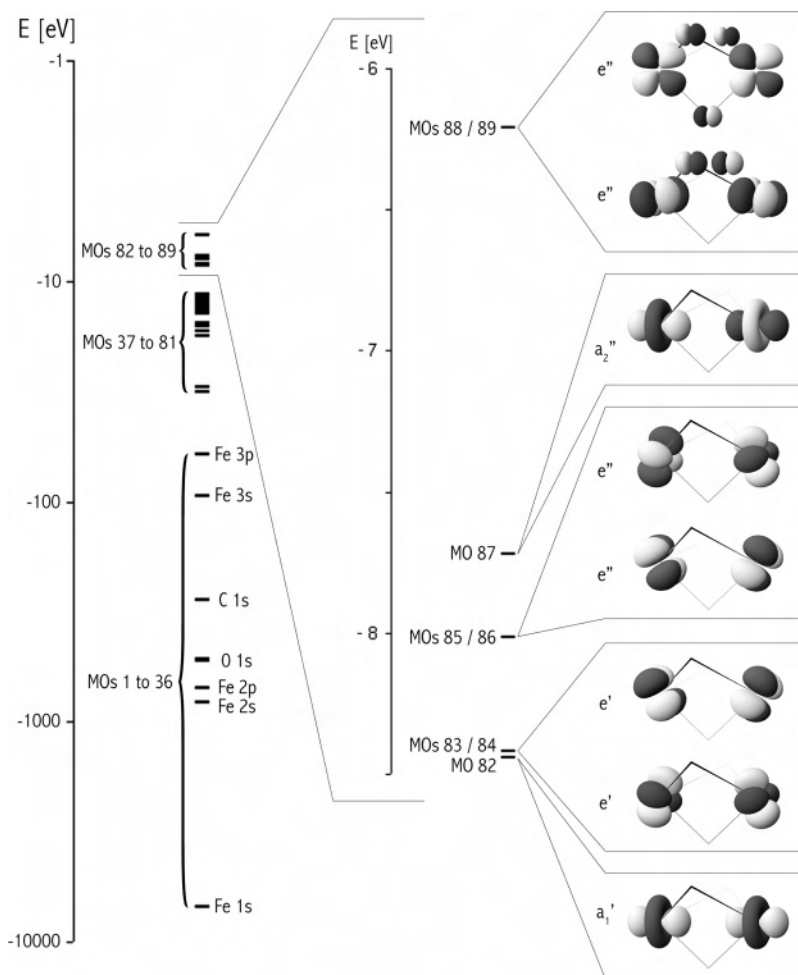
Figure 3. Eighty-nine occupied levels of Fe$_2$(CO)$_9$ in the energy scale of the DFT calculations, together with the sketches of the eight highest frontier MOs.
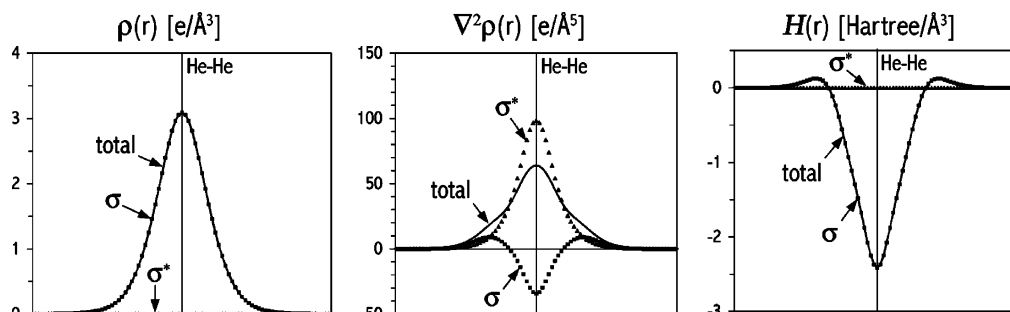

Figure 4. Total densities (solid lines) and orbital contributions (dotted lines) along a 2-fold axis of a He$_2$ model system, with a fixed separation of 75 pm.

(r_c) is maximized with a large positive value at the bcp (solid line). Consequently, a repulsive force is active between the atoms.

The Fe$_2$(CO)$_9$ molecule is now reconsidered in view of the ideal He$_2$ system, because in this case the strong metal−bridge bonds maintain a short Fe−Fe separation. Thus, σ MO 82 justifies the concentration of electron density at the bcp and the correspondingly negative value of $H(r)$. The trends of the Laplacian also become clearer (two central boxes in Figure 2). First of all, it turns out that the non-insignificant depletion at the bcp (positive minimum of the total $\nabla^2\rho(r_c)$) is largely due to the lower core MOs and only minimally to the frontier ones (82−89). The latter cause some depletion between the bridging CO ligands but not at the

Fe−Fe bcp, where the contribution to $\nabla^2\rho(r_c)$ is almost zero. In particular, the concentration due to the σ MO 82 is not overcompensated by the depletion due to σ^* MO 87, as it occurs in the He$_2$ case. The ineffectiveness of MO 87 in determining, together with MO 82, an effective electron-pair repulsion between the two metal centers agrees with the previous qualitative interpretation[20] that this a$_2$'' level is somehow involved in the formation of the sixth Fe−(CO)$_{bridge}$ bond, which adapts to such a symmetry. Indeed, the picture, which results for MO 87 (Figure 5), shows some small but critical CO π^* contributions, which mitigates the charge depletion along the Fe−Fe vector. Thus, the closed-shell interaction attributable to MO pair 82/87 has a small amount of shared-shell character. In the economy of the global MO

Figure 5. Shape of MO 87 (a_2"), which highlights a nonzero orbital contribution from the CO bridges.

architecture, even a minimum amount of back-donation helps to reduce the electron-pair repulsion, thus gaining some direct Fe−Fe bonding character. This viewpoint seems to emerge clearly from the orbital partitioning analysis.

The present strategy could also be helpful for gaining deeper insight into other complex bonding problems for which basic AIM analysis is not always decisive. For instance, bonding interactions between a He atom and a hosting adamantane cage are highlighted by the presence of the appropriate bcp's, but this seems in contrast with the endothermicity of the inclusion process.[38,39] Probably, the picture is not very dissimilar from that outlined above for the hypothetical He_2 system, where a He−He bcp coexists with a distinct repulsive interaction.

Conclusions

Although only the *total* molecular electron density $\rho(r)$ and its associated magnitudes $\nabla^2\rho(r)$ and $H(r)$ are quantum mechanically strictly defined, their partitioning in terms of single or grouped MO contributions is conceptually appropriate and useful. The AIM/MO combined approach contains some general qualitative aspects, which can be fruitfully exploited from the chemical point of view. Electron

density orbital partitioning is shown to be a valuable tool for interpreting global charge density distributions in terms of the MO architecture, which is the basic scheme used by chemists to understand electronic structure and bonding properties. In particular, the contributions of single or grouped MOs to the concentration or depletion of the charge density in a specific space region can be evaluated, thus quantifying the qualitative but intuitive picture of local bonding or antibonding character usually derived from typical MO drawings.

The potentiality of the approach has been demonstrated by investigating the bonding properties in the bridging moiety of $Fe_2(CO)_9$. It turns out that the questioned Fe−Fe bond is not critically related to the existence or the lack of the corresponding bcp, because this appears to be dependent on the computational details (basis sets and functionals), but to a specific interaction between d orbitals. Figure 2 clearly shows only a marginal variation of the *total* electron density around the Fe−Fe midpoint (leading to either a bcp or a ccp), but strong curvatures are obtained for different MO groups and the relevant individual MOs. Therefore, the information derived from the latter is not so dependent on the computational details as it is the nature of the critical point. The result, which emerges from the integration of complex theoretical approaches, confirms a previous interpretation[20] based only on the rigorous application of the symmetry and functional properties of the individual MOs[40] obtained from the highly approximated EHMO method.[41]

(38) Haaland, A.; Shorokhov, D. J.; Tverdova, N. V. *Chem.−Eur. J.* **2004**, *10*, 4416−4421, 6210.

(39) Bader, R. F. W.; Fang, D.-C. *J. Chem. Theory Comput.* **2005**, *1*, 403−414.

(40) Mealli, C.; Proserpio, D. M. *J. Chem. Educ.* **1990**, *67*, 399−402.

(41) Hoffmann, R.; Lipscomb, W. N. *J. Chem. Phys.* **1962**, *36*, 2179−2189, 3489−3493.